Transport Properties and Radiation Production in Plasmas with Sub-Larmor-Scale Magnetic Turbulence

By

Brett D. Keenan

Submitted to the Department of Physics and Astronomy and the
Faculty of the Graduate School of the University of Kansas
in partial fulfillment of the requirements for the degree of
Master of Science

Mikhail V. Medvedev, Chairperson

Committee members

Thomas E. Cravens

Gregory H. Rudnick

Date defended: December 05, 2012

The Thesis Committee for Brett D. Keenan certifies
that this is the approved version of the following thesis :

Transport Properties and Radiation Production in Plasmas with Sub-Larmor-Scale Magnetic Turbulence

Mikhail V. Medvedev, Chairperson

Date approved: December 05, 2012

Abstract

Kinetic streaming instabilities, such as the Weibel instability, occur in various HED plasma setups. Such instabilities generate strong (sub-equipartition) magnetic fields which reside at small, sub-Larmor scales. Efficient electron acceleration to relativistic energies is not uncommon in such environments. Spectra of radiation emitted by these relativistic electrons can deliver a wealth of information about the internal structure of such "Weibel turbulence". The small-scale fields simultaneously drive the particle transport via pitch-angle diffusion. Both effects are related and can be used to diagnose the plasma state. We study such a relation between transport and radiation in sub-Larmor-scale turbulence via numerical simulations and analysis.

Acknowledgements

I would like to thank Dr. Mikhail V. Medvedev for his instrumental instruction and guidance.

This research is supported by the DOE grant DE-FG02-07ER54940 and the NSF grant AST-1209665.

Contents

List of Figures

Chapter 1

1.1 Introduction

HED (high-energy density) astrophysical plasmas, and laboratory plasmas alike, are very often driven toward turbulent behavior via kinetic streaming instabilities. In particular, the *Weibel instability* (Weibel [7]; Fried [8]) is implicated in the formation of plasmas with sub-Larmor-scale (or small-scale) magnetic turbulence. This instability is also known as the *current filamentation instability* (which is a more accurate description of the phenomenon). The Weibel instability begins with a homogeneous distribution of particles with an anisotropic distribution in velocity (with no net current). This state then rapidly evolves, given an initial electromagnetic field perturbation, into the formation of opposing current filaments that reinforce the initial perturbation field – giving rise to strong electromagnetic fields that live on small-scales [6]. Environments favorable to the formation of Weibel-like instabilities include Gamma-ray bursts, relativistic pulsar winds, supernovae shocks, sites of magnetic reconnection, relativistic jets from quasars, plasmas generated via high-intensity lasers, and many more. All these diverse HED environments share a propensity for the development of spontaneous magnetic fields [6]. The generation and evolution of the Weibel instability has been studied extensively with particle-in-cell (PIC) codes which agree very closely with theory [6]. An example of the complicated magnetic fields that emerge from the Weibel instability can be seen in Figure 1.1. This plot, obtained from Medvedev, Silva, Kamionkowski [9], shows the three-dimensional structure of the self-generated magnetic field that originates from the

saturated non-relativistic Weibel instability. PIC simulations additionally reveal, in confirmation of theory first developed by Medvedev & Loeb [10], the role of the Weibel instability in collisionless relativistic shocks – like those believed to be created in gamma-ray burst (GRB) events. These shocks are "collisionless" because the scale of the shock system is much smaller than the coulomb mean-free-path. The structure of such shocks can be seen Figure 1.2, which was obtained from PIC simulations from Spitkovsky [11]. As Figure 1.1 indicates, the structure of the Weibel generated magnetic field is quite turbulent."Weibel Turbulence" leads to radiation that differs from *synchrotron. radiation*. This radiation, known as *jitter radiation*, reveals a great deal about the underlying magnetic field that produces it [1][5][6], as does the transport of electrons via pitch-angle diffusion. In fact, the radiative and transport properties are closely related; exposing, for that matter, much information about the plasma state. An elucidation is in order. To that end, we first turn our attention to pitch-angle diffusion in small-scale magnetic turbulence.

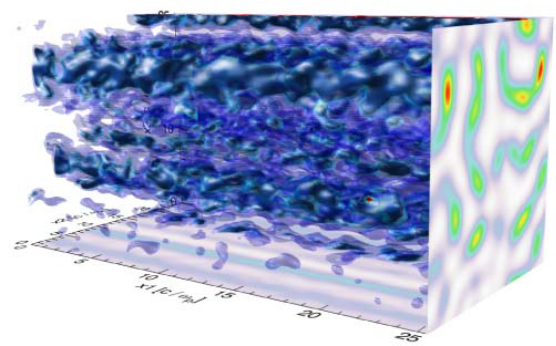

Figure 1.1: The magnetic field of the non-relativistic Weibel instability at saturation (with periodic boundary conditions). The energy density of the field is indicated by the blue iso-surfaces. The magnitude of B^2 along the x1-direction is the x2-x3-plane projection. Peaks in B^2 are indicated with red.

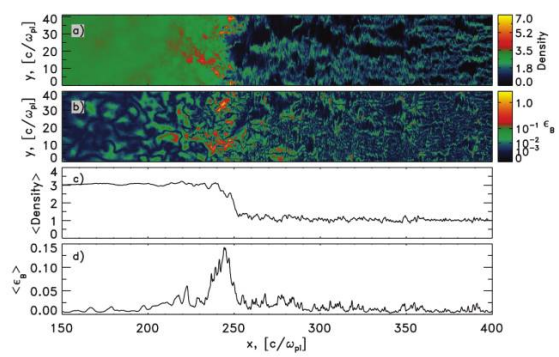

Figure 1.2: Profile of a collisionless relativistic shock, obtained from 2D PIC simulations. Adapted from Spitkovsky.

1.2 Pitch-Angle Diffusion in Small-Scale Magnetic Turbulence

If an electron moves through a non-uniform, inhomogeneous, random, small-scale magnetic field (i.e. magnetic micro-turbulence), then the electron's velocity vector will vary stochastically. This leads to, generally, random trajectories. Figure 1.3 shows several trajectories of electrons

moving through Weibel generated turbulence (once again, obtained from PIC simulations). We say that the field is "small-scale" because the electron's Larmor radius, $\rho_e = \gamma m_e c^2/eB_\perp$ (where γ is the electron's lorentz factor, m_e is the electron mass, c is the speed of light, e is the electric charge, and $B_\perp$ is the component of the magnetic field perpendicular to the electron's velocity vector) is greater than, or comparable to, the magnetic field correlation scale, λ_B (i.e. $\rho_e \geq \lambda_B$). Taking the approach of Medvedev [1] and Landau & Lifshitz [2], the deflection angle of the velocity (with respect to the particle's initial direction of motion) can be estimated by noting that the change in the electron's transverse momentum is $\sim F_L\tau$, where F_L is the transverse Lorentz force, and τ is the transit time. The transit time is the duration of time over which the particle's velocity is significantly altered. In other words, τ is the time required to traverse a length of λ_B (the scale of the field's inhomogeneity). Given the ultrarelativistic limit ($\gamma \gg 1$), $\tau \sim \lambda_B/c$. The particle's total momentum is, likewise, $p \sim \gamma m_e c$. Since $F_L \sim ec(B_\perp/c) = eB_\perp$, the change in the transverse momentum is $p_\perp \sim F_L\tau \sim eB_\perp\lambda_B/c$. The deflection angle (or, pitch-angle) is $\alpha = sin(p_\perp/p)$. An ultrarelativistic electron will only experience small deviations to its original path. Consequently, $sin(p_\perp/p) \approx p_\perp/p$. Thus, $\alpha \sim eB_\perp\lambda_B/\gamma m_e c^2$. If this process is, indeed, diffusive then there should exist a linear relationship between time, t and $\langle\alpha^2\rangle$ (the average square pitch-angle) of an ensemble of electrons. In other words:

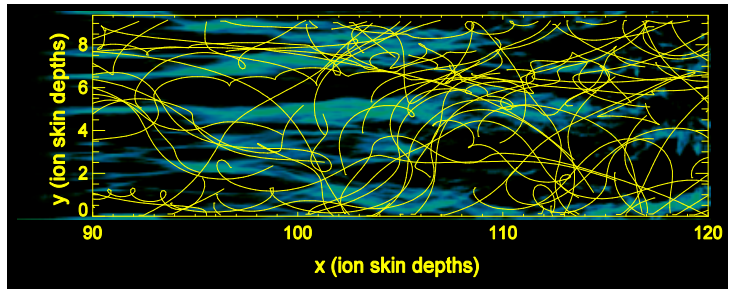

Figure 1.3: Trajectories of particles (yellow curves) moving through Weibel turbulence. A map of the density filaments produced in 2D PIC simulations is overlaid (in blue). From: C. Hededal, Ph.D. thesis, (2005) [12].

$$\langle\alpha^2\rangle \propto D_{\alpha\alpha}t, \tag{1.1}$$

where $D_{\alpha\alpha}$ is the pitch-angle diffusion coefficient. Recalling the characteristic time scale $\tau \sim \lambda_B/c$, Eq. (1.1) implies that:

$$\alpha^2 \sim D_{\alpha\alpha}\tau \sim D_{\alpha\alpha}\lambda_B/c \tag{1.2}$$

Substituting $\alpha \sim eB_\perp\lambda_B/\gamma m_e c^2$ into Eq. (1.2) gives:

$$D_{\alpha\alpha} \sim \left(\frac{e^2}{{m_e}^2 c^3}\right)\frac{\lambda_B}{\gamma^2}\langle B^2\rangle, \tag{1.3}$$

where an average square magnetic field, $\langle B^2\rangle$ has been substituted for $B_\perp^2$. Thus, Eq. (1.3) shows that the pitch-angle diffusion coefficient depends upon the statistical character of the magnetic field.

1.3 Radiation From Relativistic Particles in Small-Scale Magnetic Turbulence

From the Liénard-Wiechart (retarded) potentials for a relativistic charged particle, one can obtain the radiative spectral energy, dW per unit frequency, $d\omega$ and per unit solid angle, $d\Omega$ as [3]:

$$\frac{d^2W}{d\omega d\Omega} = \frac{e^2}{4\pi c^2}\left|\int_{-\infty}^{\infty}\frac{\hat{n}\times[(\hat{n}-\beta)\times\dot{\beta}]}{(1-\hat{n}\cdot\beta)^2}e^{i\omega(t'-\hat{n}\cdot r(t')/c)}\,\mathrm{d}t'\right|^2, \tag{1.4}$$

where $\mathbf{r}(t')$ is the particle's position at the retarded time t', $\hat{n}$ is the unit vector pointing from $\mathbf{r}(t')$ to the observer, $\beta \equiv v(t')/c$, and $\dot{\beta} \equiv \dot{v}(t')/c$. The radiation from an ultrarelativistic charge is beamed in a cone with a narrow angle of $\Delta\theta \sim 1/\gamma$. For an ultrarelativistic electron moving in a random magnetic field, the ratio of the particle deflection angle to the beaming angle is given by [1]:

$$\frac{\alpha}{\Delta\theta} \sim \frac{eB_\perp\lambda_B}{m_e c^2} \sim 2\pi\frac{e\langle B^2\rangle^{1/2}}{k_B m_e c^2} \equiv \delta. \tag{1.5}$$

For convenience, we have defined δ (the *jitter parameter*) in terms of a characteristic wave number, k_B of the magnetic field ($\lambda_B \sim k_B^{-1}$), and the average squared field [1][4]. When $\delta \gg 1$ (i.e.

$\alpha \gg \Delta\theta$), the beaming angle is small compared to the deflections. An onlooking observer would see radiation from only short intervals of the electron's trajectory (i.e. whenever the trajectory is near the line-of-sight). This radiation is similar to synchrotron radiation. However, if $\delta \ll 1$, the electron's deviations are very small compared to its beaming angle. As a result, the radiation is seen by a line-of-sight observer throughout the entire trajectory of the particle (see Figure 1.4) [1][2]. Thus, the resulting radiation spectrum is distinct from that produced by synchrotron radiation.[0]

This is the previously mentioned *jitter radiation* [1][4]. The characteristic frequency of jitter radiation can be estimated by considering the electron's acceleration. The correlation scale λ_B', as seen in the electron's rest frame, is related to λ_B in the lab frame by a Lorentz transformation (i.e. $\lambda_B' \sim \lambda_B/\gamma$). Again, the electron's transverse accelerations occur only significantly over the length scale of λ_B. This corresponds to a time scale, in the electron's frame, of $\tau' \sim \lambda_B'/c$. Thus, the radiation emitted by the electron has a characteristic frequency, in the electron's rest frame, of $\omega' \sim 2\pi/\tau' \sim 2\pi c/\lambda_B' \sim 2\pi\gamma c/\lambda_B$. Transforming back to the lab frame picks up another factor of γ, giving the characteristic frequency of $\omega_j \sim 2\pi c\gamma^2/\lambda_B$, or [1]:

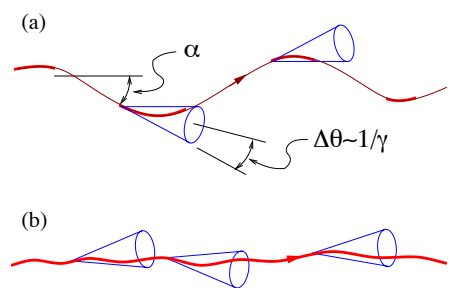

Figure 1.4: (a) – $\alpha \gg \Delta\theta$, radiation is only seen along periodic segments of the path. (b) – $\alpha \ll \Delta\theta$, radiation is seen from the entire trajectory. From Medvedev [6].

$$\omega_j \sim \gamma^2 k_B c, \tag{1.6}$$

with a substitution of the characteristic wave number, k_B. Thus, we can see that the resultant particle radiation spectrum depends on the spectral characteristics of the turbulent magnetic field. Furthermore, the field structure is, more generally, revealed by the shape of the radiation spectrum. To see this, we adopt a particular magnetic field spectral distribution. One of the simplest is given by a power law; simpler still is a power law that is isotropic in k-space. This power law has the

[0] It is worth noting that the total radiated power of jitter radiation is actually identical to that of synchrotron. The formula: $dW/dt = (2/3)r_e{}^2 c\gamma^2 B_\perp^2$, where $r_e = e^2/m_e c^2$ is the classical electron radius, works just as well – so long as $B_\perp^2$ is replaced by $\langle B_\perp{}^2\rangle$ [1].

functional form:

$$|\mathbf{B}_{\Omega,\mathbf{k}}|^2 \propto k^{-\mu}, \tag{1.7}$$

where $\mathbf{B}_{\Omega,\mathbf{k}}$ is the Fourier transform of the magnetic field in space and time, Ω is the spectral frequency, $\mathbf{k}$ is the wave vector, and μ is a positive real number. Notice that this distribution is independent of time and wave vector direction. We further impose the condition that $|\mathbf{B}_{\Omega,\mathbf{k}}|^2 = 0$, if k is outside a chosen range of $[k_{min}, k_{max}]$. An isotropic, static magnetic turbulence of this sort is expected to arise in the advanced stage of the non-linear evolution of the Weibel instability [6]. Medvedev et al. [4] showed that the angle-averaged[1] radiation spectrum (i.e. Eq. (1.4) integrated over $d\Omega$) of an ultrarelativistic electron, with $\delta \ll 1$, will be given by two power laws, the first of which is flat ($I_\omega \propto \omega^0$) up to E_{peak} (where $\omega \sim \omega_j \equiv \gamma^2 k_{min} c$). The second power law follows after ω_j as $I_\omega \sim \omega^{-\mu+2}$ [4]. In general, the shape of the radiation spectrum depends upon the magnetic field spectral distribution (which need not be a simple power law) and/or the distribution of particles. Thus, by observing the radiation spectrum, one can probe the structure of the magnetic turbulence that generates it.

[1] Alternatively, one can obtain the same spectrum by averaging Eq. (1.4) for an isotropically distributed, mono-energetic ensemble of electrons. This was the procedure employed in our numerical simulations.

Chapter 2

2.1 Radiation and Diffusive Transport as a Diagnostic Test of the Plasma State

As indicated in the previous chapter, the radiative and diffusive properties of small-scale magnetic turbulence are closely related. The two are connected via their mutual relation to the statistical properties of the magnetic field (e.g. $\langle B^2 \rangle$ and λ_B). In principle, $\langle B^2 \rangle$ and λ_B can be obtained either via an examination of the radiation spectrum, or by measuring the pitch-angle diffusion coefficient. Ideally, a comparison between the two could act as a test of self-consistency. By obtaining the same result via two distinct methods, we can be doubly assured that we know what is happening in our plasma.

There is one physical problem, in particular, where this interconnection plays a vital role in the problem's resolution – Gamma-ray bursts (GRBs). Although observational data on GRBs has been plentiful in recent years, much is still unknown about the physics behind GRB emissions. The "standard model" of GRBs posits that radiation is produced at collisionless shocks by relativistic outflows (these outflows originate from some sort of "progenitor" event). The energy of this outflow is converted in the shock into magnetic fields and thermal energy of electrons. These electrons, subsequently, emit the radiation which is the observational signature of the GRB. The radiation from these electrons is in the jitter regime, as the scale of inhomogeneity of the generated magnetic fields is large compared to the typical electron Larmor radius. The particle acceleration

is mediated by either first or second order Fermi acceleration. A particle can be accelerated by successive crossings of the shock, or it could proceed by repeated turbulent scatterings. The turbulent scattering, as already discussed, can be driven by small-scale electromagnetic fields (like those produced by a Weibel-like instability). As previously noted, the Weibel instability plays a major role in collisionless shocks. Consequently, the Fermi acceleration of particles from these events is likely driven by turbulent, small-scale electromagnetic fields. If this is the case, then the acceleration mechanism should be described by the diffusion coefficient in the upstream and downstream of the shock. This is generally true of any acceleration region (not simply from shocks); the transport properties are indicated by the diffusion coefficient. Direct observations of the pitch-angle diffusion coefficient are not possible in the astrophysical environment. Typically, certain assumptions are made (e.g. that the acceleration is governed by Bohm diffusion) to estimate the diffusion coefficient, but there has not been a direct way to obtain it – until now. By exploiting the interconnection between diffusive transport and radiation in this magnetic micro-turbulent environment, we can obtain the pitch-angle diffusion coefficient directly from the radiation spectra (which is observationally available). With this, then, we will have a more complete picture of the particle acceleration mechanism, and thus the GRB phenomenon itself [6].

Our original intent was to demonstrate, via simulations of particles in magnetic turbulence, that the diffusive and radiative properties of these plasmas are, indeed, related as we believe. We did these simulations solely from first principles. The physical system simulated is an infinite space. This space is divided into “cubes", each with an identical turbulent magnetic field inside. Relativistic electrons are flying around; there is no significant interaction between them. Thus, each electron’s motion is solely determined by the Lorentz force equation given by:

$$\frac{d\mathbf{v}}{dt} = -\frac{e}{\gamma m_e}\beta \times \mathbf{B} \tag{2.1}$$

So, by solving this equation of motion for each particle, $\langle \alpha^2 \rangle$ can be calculated. Then, to obtain the diffusion coefficient, $\langle \alpha^2 \rangle$ is plotted as a function of simulation time. Likewise, the radiation

spectrum for each particle is given by Eq. (1.4). Finally, the total spectrum can be obtained by adding the spectra of each particle (this can either be done “coherently" or “incoherently"). In the next section, I will address specific details of the numerical implementation.

2.2 Numerical Implementation

The simulation has two principle stages. First, the turbulent magnetic field must be generated from a given spectral distribution in Fourier space. This field is created on a lattice that is then interpolated, so that a “continuous" field is represented. The second stage then involves the numerical solution of the equation of motion for each particle, from which $\langle \alpha^2 \rangle$ and the radiation spectra are obtained. We will first turn our attention to the generation of the magnetic field.

We opted to generate the magnetic field in Fourier space. This representation is convenient for two reason. For one, it is simpler to specify a particular spectral distribution in Fourier space directly, rather than attempting to find a field in real space that has a particular spectral distribution. Secondly, if this random field is to be a physically realizable magnetic field, then its divergence must be zero. Producing a divergenceless field in Fourier space is far simpler than generating one in real space. This is because, in Fourier space:

$$\nabla \cdot \mathbf{B} \rightarrow i\mathbf{k} \cdot \mathbf{B}_{\mathbf{k}}, \tag{2.2}$$

where $\mathbf{k}$ is the wave vector associated with the Fourier representation of the magnetic field, $\mathbf{B}_{\mathbf{k}}$. Thus, in Fourier space, Gauss’s Law simply becomes:

$$\mathbf{k} \cdot \mathbf{B}_{\mathbf{k}} = 0. \tag{2.3}$$

This condition can be imposed by an application of the Gram-Schmidt process to each $\mathbf{k}$, $\mathbf{B}_{\mathbf{k}}$ pair.

So, we begin with a 3-dimensional lattice of points over a box of finite length (these will then form the identical “cubes" that fill the “infinitely" sized box used in the simulation). Given this constraint, the representable wave numbers of the magnetic field range anywhere from $2\pi/L_{box}$ to the Nyquist frequency. Next, to ensure that the magnetic field is actually random, each $\mathbf{B_k}$ is oriented in a random direction, and then multiplied by a random phase factor. Furthermore, to ensure that the inverse Fourier transform of $\mathbf{B_k}$ yields a purely real $\mathbf{B}$-field, hermiticity is imposed upon the field. Prior to the inverse transform, the field must be normalized to fit a predefined spectral distribution. In our preliminary results to follow, the isotropic power law of Eq. (1.7) was chosen. In this case, each $\mathbf{B_k}$, within $[k_{min}, k_{max}]$, is normalized, such that:

$$|\mathbf{B_k}|^2 = k^{-\mu}, \tag{2.4}$$

with all other $\mathbf{B_k}$ set to zero. Once the inverse Fourier transform (performed numerically via a *Fast Fourier Transform*, or FFT) is done, the emerging real magnetic field is normalized such that $\langle B^2 \rangle$ obtains a predefined value. Finally, an interpolating function is applied to the field to cover points internal to the lattice “cubes" (i.e. in-between lattice points). Although the magnetic field given by the lattice points is divergenceless, our interpolated field may not be. To ensure that the interpolant is, likewise, divergence-free, we employed an interpolating function called a matrix-valued radial basis function. As described by McNally [5], divergence-free matrix-valued radial basis function interpolants, $\Phi(\mathbf{x})$ can be created from a radial basis function, $\phi(\mathbf{x})$ by the transformation:

$$\Phi(\mathbf{x}) = (\nabla\nabla^T - \nabla^2\mathbf{I})\phi(\mathbf{x}), \tag{2.5}$$

where $\mathbf{I}$ is the $n \times n$ identity matrix. In our simulations, a simple basis function of $\phi(\mathbf{x}) = e^{-\varepsilon r^2}$ was chosen (where ε is some predefined parameter). The resulting $\Phi(\mathbf{x})$, given by Eq. (2.5), was then used to interpolate the field intermediate to lattice points in a divergence-free manner.

The next stage in the simulation starts with the numerical solution of the equation of motion, Eq. (2.1). This was done via a fixed step 4th-order Runge-Kutta-Nyström method. Once the particle positions, velocities, and accelerations are calculated, $\langle \alpha^2 \rangle$ is straightforwardly calculated. After the pitch-angle calculation, the spectrum of each particle is calculated. Before integration, we multiplied a window function to our signal to avoid spectral leakage. We then had a choice in regard to how the total radiation spectrum is obtained. One option is to add the spectra coherently (i.e. by taking the Fourier transform of the "summed over" radiation fields of each particle). In this case, only a single integration would be needed. Alternatively, we can add the spectra incoherently (i.e. by integrating each particle's radiation field separately, and then summing the results of each integration). We chose the latter, opting to add the spectra incoherently.

An incoherent sum gives sharper spectra, but this is at a cost. Typically, Fourier transforms are done numerically via an FFT, which is $\sim \mathscr{O}(Nlog(N))$ in complexity, where N is the number of time steps. This means that the integration must be performed directly (i.e. via a Riemann sum, which is $\sim \mathscr{O}(N^2)$ in complexity). The majority of the runtime is spent on this integration. This means that the runtime scales roughly $\sim \mathscr{O}(N^2)$. Thus, we see that the run time to effect a direct integration is considerably longer than the time to perform an FFT (which requires fewer operations). Unfortunately, since the integration in Eq. (1.4) is over the retarded time (which includes a frequency-dependent exponential), an FFT cannot be easily calculated.[2] Since the particle runs are decoupled from each other, we would initially expect the total runtime to scale $\sim \mathscr{O}(N_p)$, where N_p is the number of particles. So far, these estimates have proven to be fairly decent. However, we have yet to determine more precise scalings (especially in a parallel computing environment).

[2]Of course, the integration could be performed via an FFT, in the observer's time (instead of the retarded time). Unfortunately, this route is plagued by difficulty. Two particularly serious issues concern numerical stability, and the lack of a fixed time step in the observer's time (which requires careful interpolation of particle positions, velocities, etc.).

2.3 Preliminary Results

To test our code, we set out to verify what we already knew. Namely, does the code show that radiation production and diffusion are related as we have expected? To answer this, we explored the motion of relativistic electrons in isotropic magnetic micro-turbulence. As our test must be thorough, we were sure to check our code against all the parameters. These included: the number of particles N_p, the Lorentz gamma factor of each particle γ, the magnetic field strength $\langle B^2 \rangle$, the jitter parameter δ, the size of the simulation box, the wave number range of the magnetic field spectrum, the total simulation time, and the the magnetic spectral power law exponent, μ. I will now reveal our results – one by one. First, how does our numerically obtained pitch-angle diffusion coefficient compare to the theoretical result, Eq. (1.3)? Does it depend strongly upon the number of particles used in the simulation? Figure 2.1 shows that $D_{\alpha\alpha}$ does not change considerably with increasing number of particle – as expected. Next, we tested the γ dependence. Figure 2.2 shows close agreement between the theoretical and numerical diffusion coefficients with varying Lorentz factor. $D_{\alpha\alpha}$ depends on two additional parameters – k_{min} and

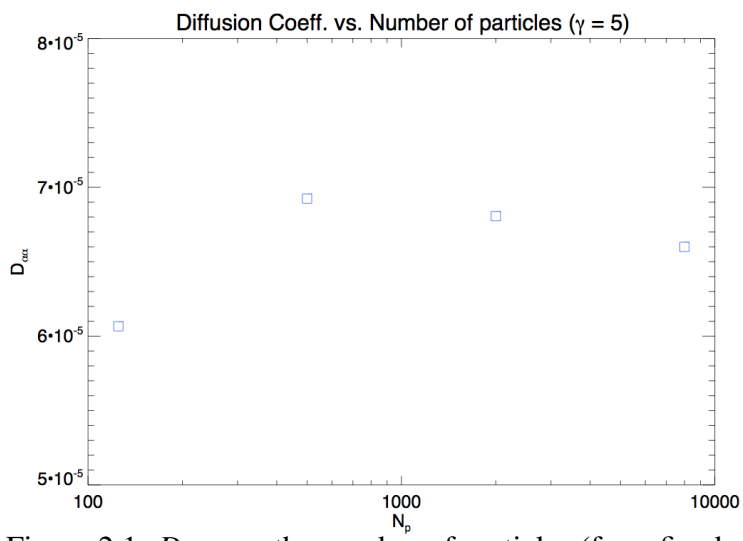

Figure 2.1: $D_{\alpha\alpha}$ vs. the number of particles (for a fixed γ, k_{min}, etc.).

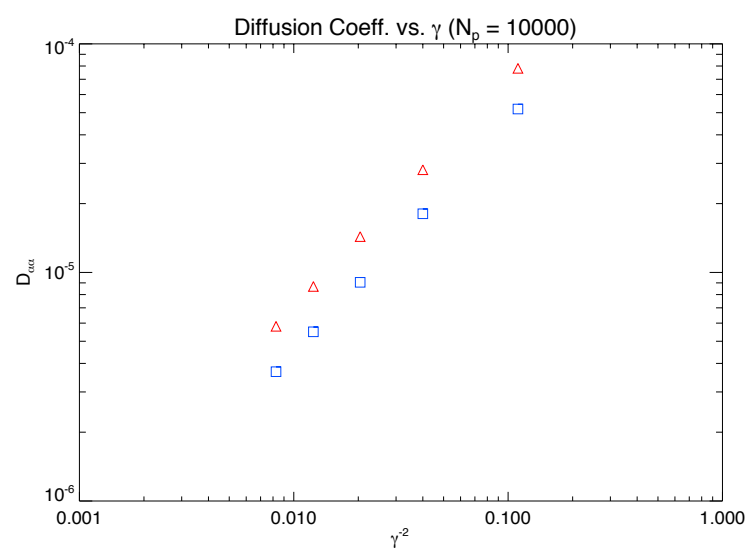

Figure 2.2: $D_{\alpha\alpha}$ vs. γ^{-2}. The "blue squares" indicate the $D_{\alpha\alpha}$ obtained directly from simulation (as the slope of $\langle \alpha^2 \rangle$ vs. time), while the "red triangles" are the "theoretical" $D_{\alpha\alpha}$.

$\langle B^2 \rangle$. Instead of plotting $D_{\alpha\alpha}$ vs. k_{min} directly, we chose to plot the diffusion coefficient vs. the frequency of E_{peak} – which is given in Eq. (1.6) – in the radiation spectrum. This was done so that we may hit home the idea that these are actually related. Figure 2.3 shows close agreement.[3] Figure 2.4 covers $\langle B^2 \rangle$; it reveals the diffusion coefficient's expected dependence.

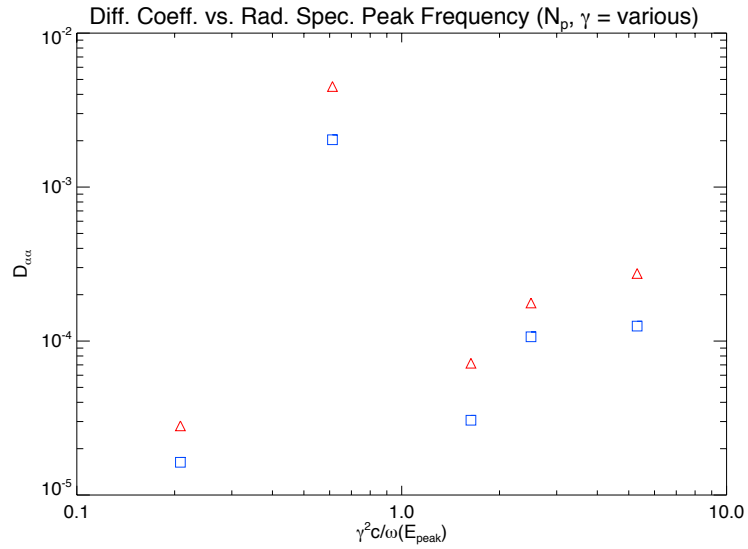

Figure 2.3: $D_{\alpha\alpha}$ vs. the frequency of E_{peak}, i.e. the frequency given by Eq. (1.6). Once again, the "blue squares" indicate the $D_{\alpha\alpha}$ obtained directly from simulation while the "red triangles" are the "theoretical" $D_{\alpha\alpha}$.

Next, we will examine the radiation spectra. To start, it was instructive to reproduce the simplest result – the radiation spectrum from a single relativistic charged particle in a uniform magnetic field. Figure 2.5 shows that our code correctly resolves this spectrum. Here, the blue curve represents the numerically resolved synchrotron harmonics (which are integer multiples of the gyrofrequency, $\omega_B = eB_\perp/m_e c$). We see a close agreement to the analytical result, indicated in red. Once we were certain that the radiation spectra are being resolved properly, we went on to the random field

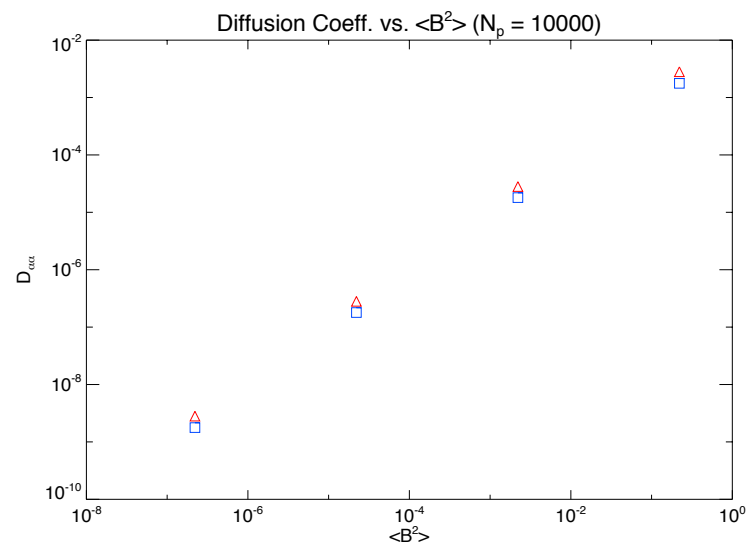

Figure 2.4: $D_{\alpha\alpha}$ vs. $\langle B^2 \rangle$. As before, the "blue squares" indicate the $D_{\alpha\alpha}$ obtained directly from simulation while the "red triangles" are the "theoretical" $D_{\alpha\alpha}$.

[3] It is worth noting that the apparent difference between the theoretical and numerical diffusion coefficients in these plots is largely due to a fixed numerical factor. We can be assured that this factor is relatively fixed, given that the difference between the numerical and theoretical results does not vary considerably from case to case.

tests. Figure 2.6 demonstrates the sharpening of the radiation spectra with increasing number of particles (note: all the following plots are arbitrarily normalized). In Figure 2.7, we confirm that the frequency of E_{peak} scales with k_{min}. One interesting feature of the spectra in Figure 2.7, however, is that the power law of ω^{-1} does not hold well for higher frequencies. We see that this "problem" continues in Figure 2.8, where we have increased the temporal resolution (allowing the resolution of higher frequencies). Figure 2.9 finally clears up the problem by showing how the spectra scale with k_{max}. There is a transition from a power law, to steep decay, near $\gamma^2 k_{max} c$. This transition denotes the maximum wave number of our magnetic field representation; thus, we expect such a cutoff. Next, we tested the gamma dependence. Figure 2.10 demonstrates that the frequency of E_{peak} scales $\sim \gamma^2$, as expected. Additionally, 2.10 shows that the *shape* of the radiation spectrum is independent of the particle's Lorentz factor. The next test was to demonstrate the μ dependence. Figure 2.11 shows that the spectral power law is $-\mu + 2$, as we had believed.

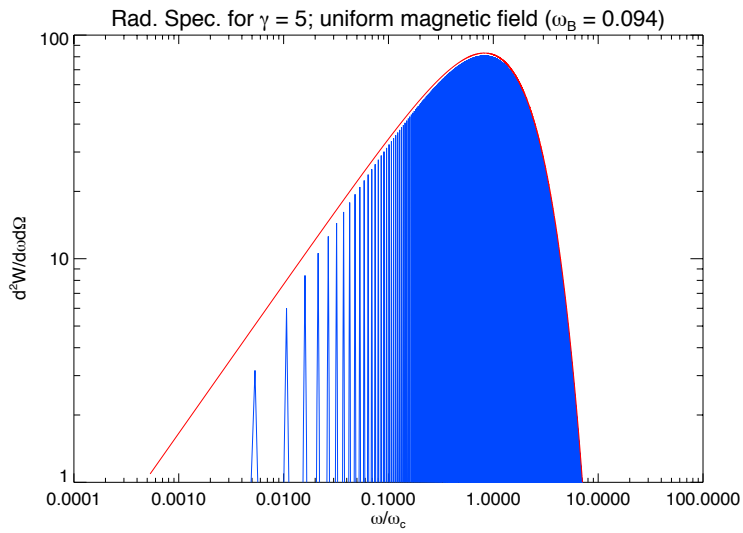

Figure 2.5: Radiation spectrum of a single relativistic charge moving through a uniform magnetic field. The numerical solution is indicated in blue. The red line is the analytical solution. Note: $\omega_B = eB_\perp/\gamma m_e c$, is the electron gyrofrequency, and $\omega_c = (3/2)\gamma^2\omega_B$, is the critical synchrotron frequency (i.e. the peak of the spectrum).

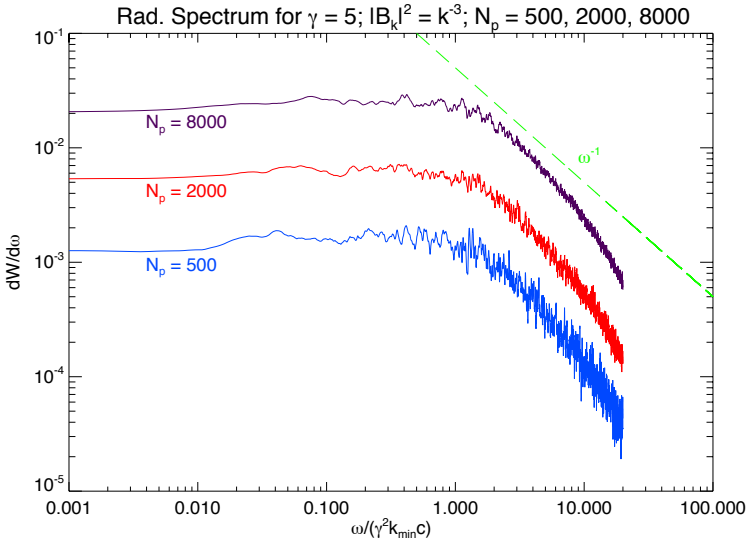

Figure 2.6: Sharpening of the radiation spectrum with number of particles, N_p.

Finally, we wished to see that the transition from the small-angle jitter regime, all the way to synchrotron-like radiation, occurs as expected. In Figure 2.12, we have superimposed spectra of increasing jitter parameter. We see that radiation is in the small-angle jitter regime for all k for which $\delta < 1$. As δ increases to values greater than unity, we make the transition from the jitter-synchrotron hybrid of the large-angle jitter regime to the pure synchrotron spectrum with its characteristic slope of $1/3$ and exponential decay beyond the synchrotron frequency [3]. Lastly, we demonstrated that the magnetic field spectral distribution is composed of independent jitter parameter scales. Recall that the magnetic field power spectrum ranges from a k_{min} to k_{max}. Consequently, there is a magnetic field "scale" associated with each k-mode. In Figure 2.13, we have divided a wave number range into the small-scale portion (i.e. all k for $\delta < 1$) and the large-scale portion (i.e. all k for $\delta > 1$). We see that the large-scale component produces a synchrotron-like spectrum (the disconnected orange line designates the typical synchrotron spectral shape), and the small-scale portion is decidedly in the small-angle jitter regime.

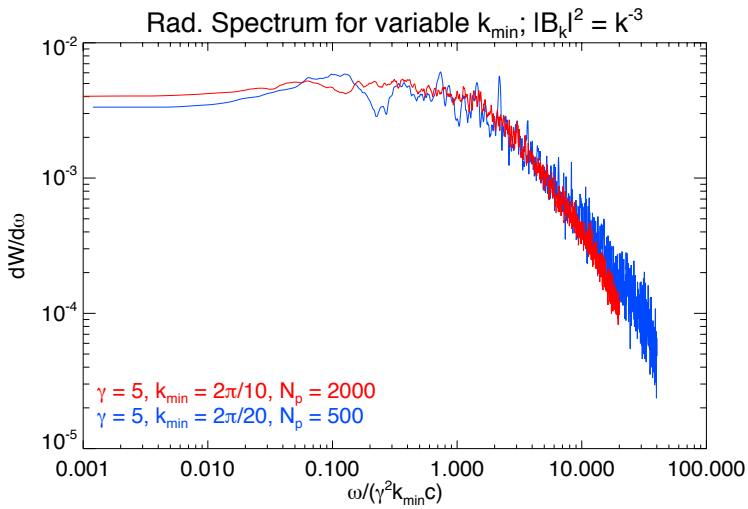

Figure 2.7: Radiation spectrum illustrating the k_{min} dependence (the two spectra differ in the k_{min} by a factor of 2).

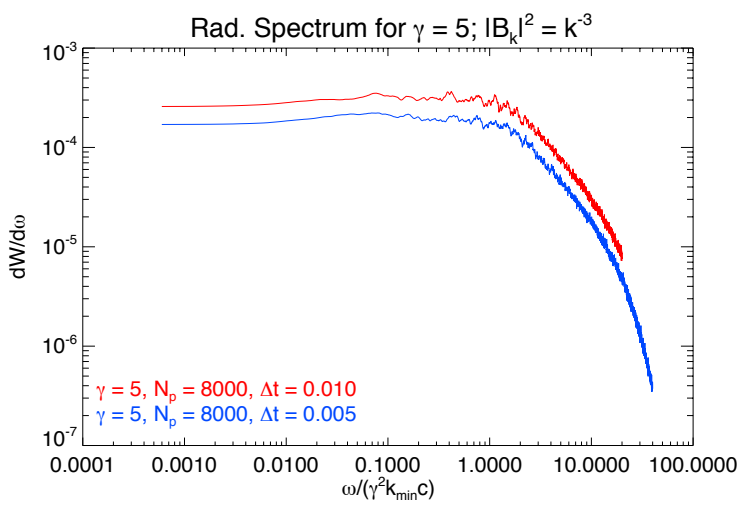

Figure 2.8: We see that the trend first noted in the previous plot continues for higher frequencies.

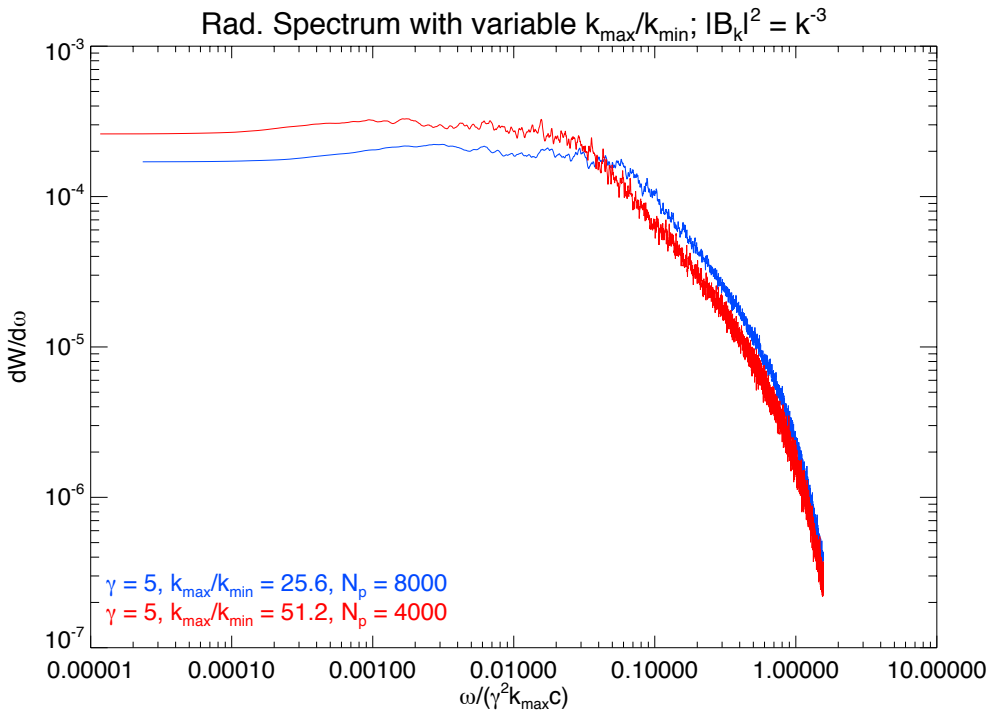

Figure 2.9: Radiation spectrum illustrating the k_{max} dependence (the two spectra differ in the k_{max} by a factor of 2). The transition from a power law of ω^{-1} to a steep drop off occurs $\sim \gamma^2 k_{max} c$, as anticipated.

Additionally, we see that the sum of the two scales produces the spectrum over the entire wave number interval – as expected, given their independence. Last – but not least – we modified Figure 2.13 to demonstrate, once more, the k_{max} dependence. The full scale interval, i.e. the interval of wave numbers that give a jitter parameter interval of $\delta \in [0.1, 4]$, should have the same k_{max} as the small-scale component, i.e. the interval of wave numbers that give a jitter parameter interval of $\delta \in [0.1, 1]$. In Figure 2.14, where we have plotted these normalized to k_{max}, we see that the two line up perfectly. This reinforces the result of Figure 2.9.

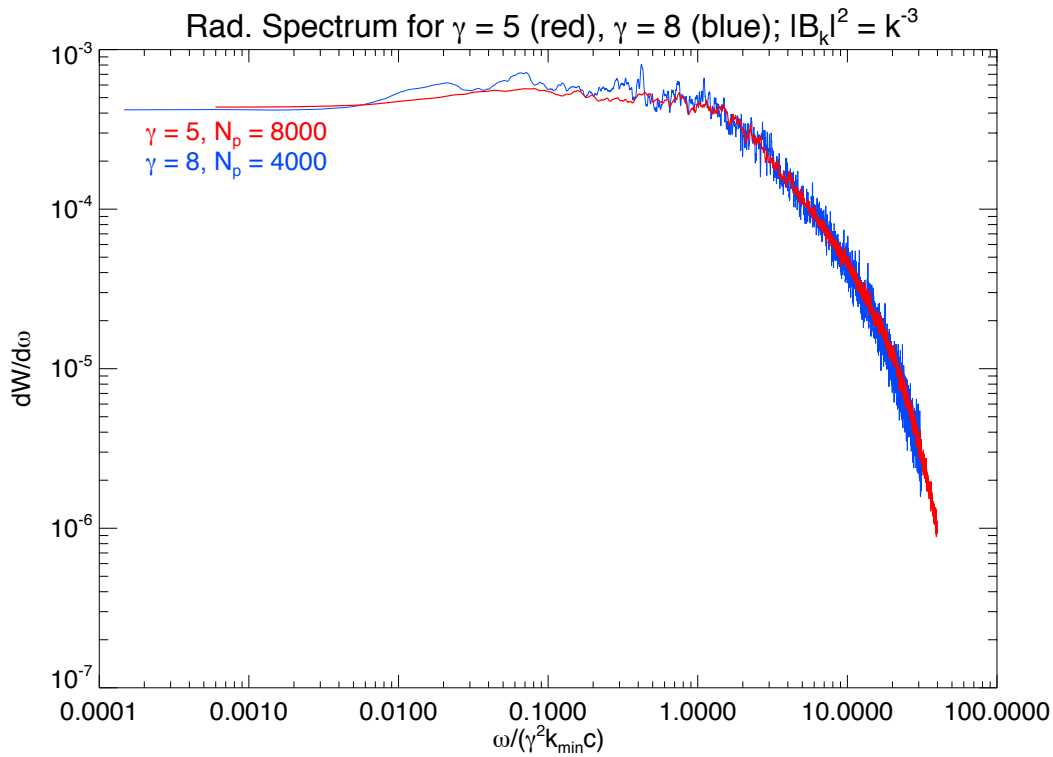

Figure 2.10: $\gamma = 5$ and $\gamma = 8$ spectra superimposed, confirming the invariance of the shape with respect to the Lorentz factor.

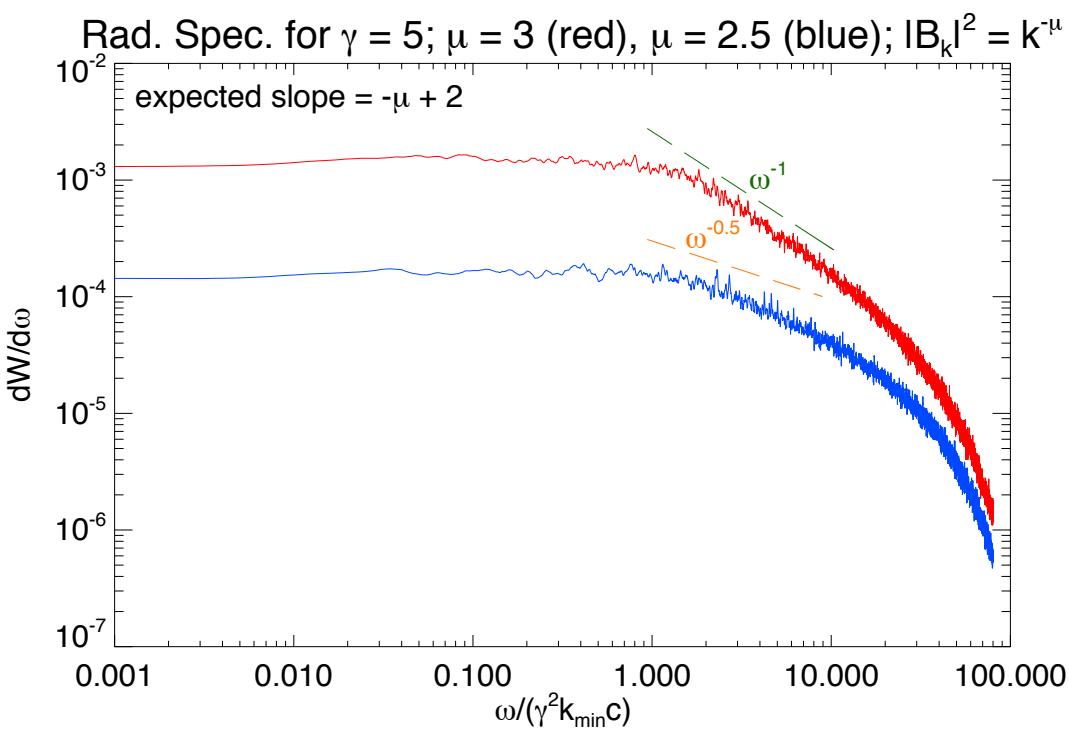

Figure 2.11: The power law following $\gamma^2 k_{min} c$ is, as anticipated, $\sim \omega^{-\mu+2}$

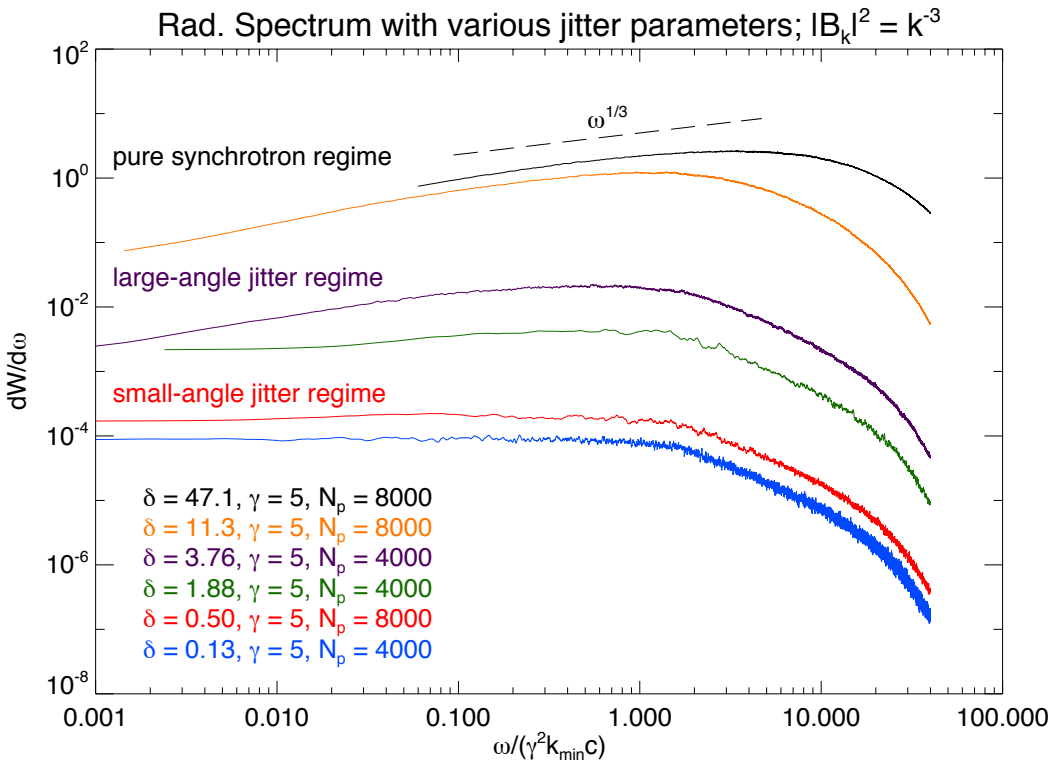

Figure 2.12: the eventual emergence of synchrotron radiation (with its distinctive 1/3 slope) as the jitter parameter, δ increases.

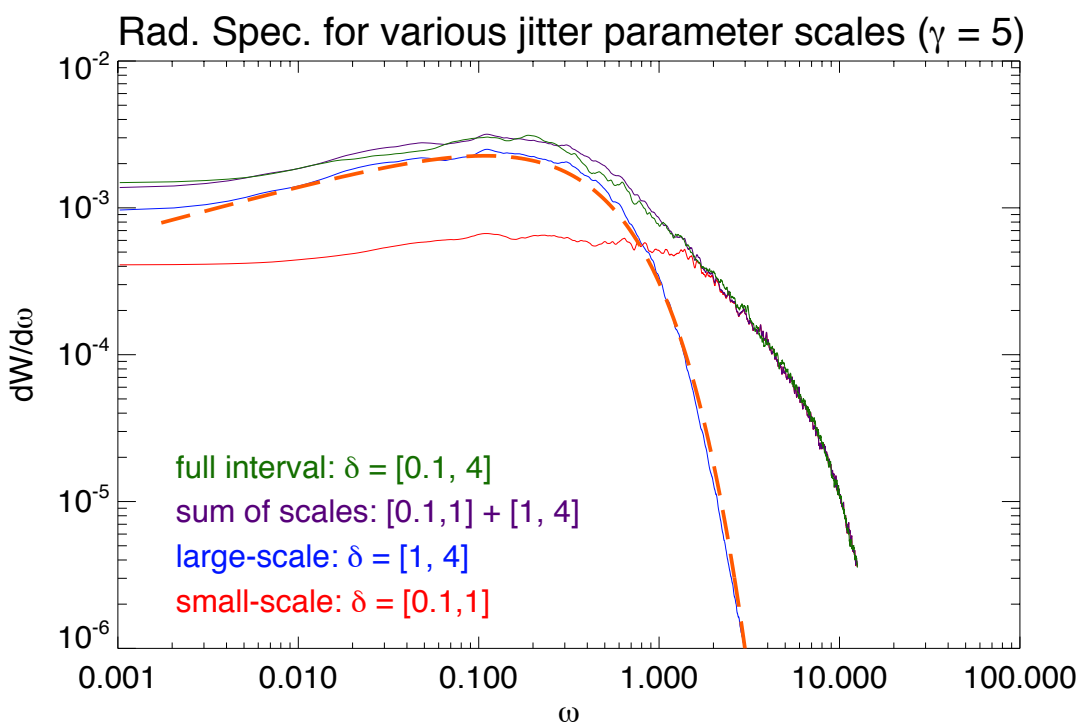

Figure 2.13: Spectrum from the small-scale field contribution ($\delta \in [0.1, 1]$) superimposed with the spectrum from the large-scale field contribution ($\delta \in [1, 4]$), their sum, and the full scale interval ($\delta \in [0.1, 4]$).

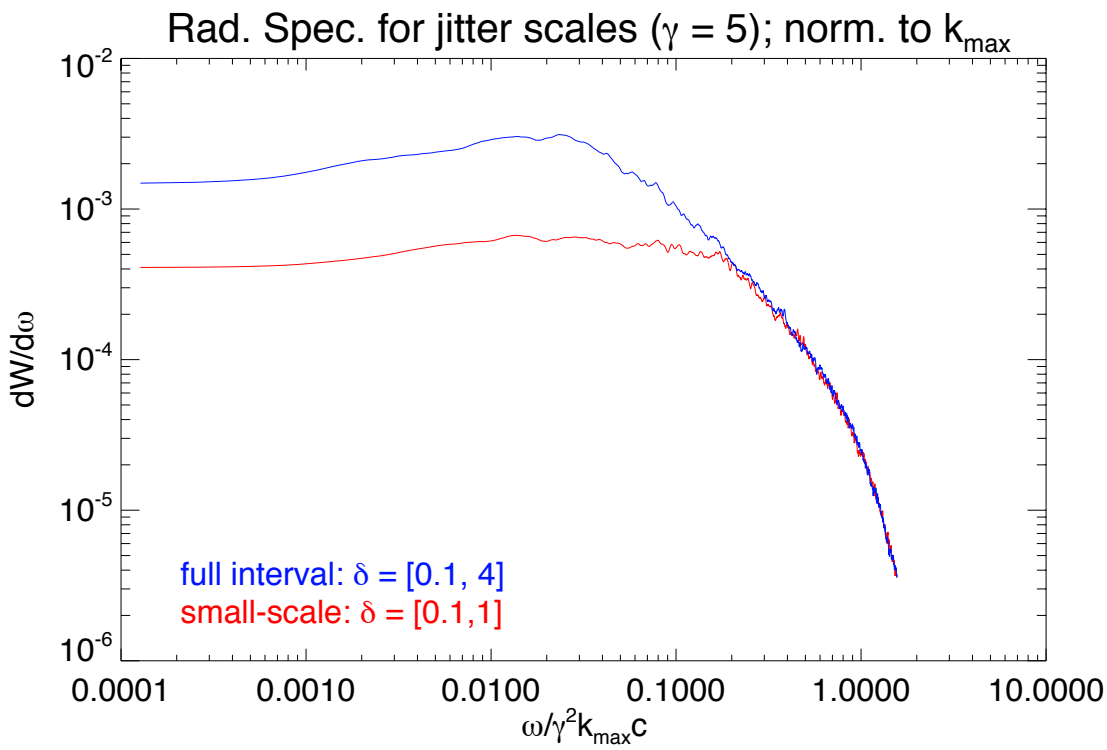

Figure 2.14: Spectrum from the small-scale field contribution, $\delta \in [0.1, 1]$, superimposed with the spectrum from the total jitter parameter interval, $\delta \in [0.1, 4]$. Here, we see the correct scaling with k_{max}.

2.4 Future Plans

We expect that this interconnection between radiation production and diffusion in magnetic turbulence holds in regimes distinct from the small-angle jitter regime. Medvedev *et. al.* [4], have made considerable progress in characterizing, what may be called, the large-angle jitter regime. In its radiative properties, this regime exhibits a sort of jitter/synchrotron hybrid. Although there is still work to be done on this, there is another regime that may be of particular interest to a certain class of laboratory plasmas. Weibel-like instabilities may produce turbulent small-scale magnetic fields in plasmas wherein subrelativistic particles play a part. Since these particles certainly do not have gamma factors much greater than unity, our earlier analysis fails. As of yet, we do not have a theory that describes this regime, but we may learn much by looking at the regime via simulation.

To explore this subrelativistic regime, we will need to apply our battery of tests once more. We will explore how the diffusive/radiative properties change with magnetic field strength, magnetic spectral distribution, particle velocity, number of particles, and any other relevant set of parameters. We expect that these simulations, like our preliminary tests, will be computationally expensive. We will, once more, require supercomputer use. Fortunately, since the total simulation time required is proportional to the γ of our particles, we will not likely require as much in computational resources. Additionally, the lack of relativistic beaming of the radiation will allow the resolution of finer spectra with fewer particles. We expect that our initial scalings will hold fairly well, even in this regime. Once again, thorough testing will be required to obtain more precise scalings.

2.5 Conclusions

With much confidence, we can conclude that the structure of sub-Larmor-scale magnetic turbulence is readily identified by inspecting the transport and radiation production of relativistic particles moving through it. Although nothing conclusive can be said of the unexplored regimes, we are assured this interconnection holds generally. We will shed light on the matter soon.

Bibliography

[1] Mikhail V. Medvedev (2000) ApJ 540 704

[2] Landau L. D., Lifshitz E. M. 1975, *The Classical Theory of Fields, Course of Theoretical Physics, Vol. 2* (New York : Pergamon)

[3] Jackson, J. D. 1999, *Classical Electrodynamics* (3rd. New York:Wiley)

[4] Medvedev M. V., Trier Frederiksen J., Haugboelle T., Nordlund A. (2010) arXiv:1003.0063

[5] McNally C. P. (2011) arXiv:1102.4852v1 [astro-ph.IM]

[6] Mikhail V. Medvedev (private communication, 2012).

[7] Weibel, E. S. 1959, Spontaneously Growing Transverse Waves in a Plasma due to Anisotropic Velocity Distribution, PRL, 2, 83

[8] Fried, B. D. 1959, Mechanism for Instability of Transverse Plasma Waves, Phys. Fluids, 2, 337

[9] Medvedev, M. V., Silva, L. O., Kamionkowski, M. 2006, Cluster magnetic fields from large-scale-structure and galaxy-cluster shocks, ApJL, 642, L1

[10] Spitkovsky, A. 2008, ApJL, 673, L39

[11] Hededal, C.B. 2005, PhD thesis, Niels Bohr Institute, Copenhagen; arXiv:astro-ph/0506559